A compact, high performance atomic magnetometer for biomedical applications

2013 Phys. Med. Biol. 58 8153

(http://iopscience.iop.org/0031-9155/58/22/8153)

IOP Publishing Physics in Medicine and Biology

Phys. Med. Biol. **58** (2013) 8153–8161 doi:10.1088/0031-9155/58/22/8153

A compact, high performance atomic magnetometer for biomedical applications

Vishal K Shah[1] **and Ronald T Wakai**[2]

[1] QuSpin Inc., Westminster, CO 80021, USA
[2] University of Wisconsin, Madison, WI 53705, USA

E-mail: vshah@quspin.com

Received 9 July 2013, in final form 21 October 2013
Published 7 November 2013
Online at stacks.iop.org/PMB/58/8153

Abstract

We present a highly sensitive room-temperature atomic magnetometer (AM), designed for use in biomedical applications. The magnetometer sensor head is only $2 \times 2 \times 5$ cm^3 and is constructed using readily available, low-cost optical components. The magnetic field resolution of the AM is $<$10 fT Hz$^{-1/2}$, which is comparable to cryogenically cooled superconducting quantum interference device (SQUID) magnetometers. We present side-by-side comparisons between our AM and a SQUID magnetometer, and show that equally high quality magnetoencephalography and magnetocardiography recordings can be obtained using our AM.

(Some figures may appear in colour only in the online journal)

1. Introduction

Biomagnetism entails the study of extremely weak magnetic fields originating from biological systems, including the human body. The most important and most extensively investigated biomagnetism signals are the magnetoencephalogram (MEG) and the magnetocardiogram (MCG), which are the magnetic analogs of the EEG and ECG, respectively. The detection of biomagnetism was enabled by the advent of the superconducting quantum interference device (SQUID) magnetometer in the 1960s (Weinstock 1996), and SQUIDs are still the most sensitive commercially available magnetic field detectors. In recent years, however, atomic magnetometer (AM) technology has advanced significantly, and laboratory prototypes with sensitivity exceeding that of SQUID magnetometers have been demonstrated (Dang *et al* 2010). A major advantage of the AM over SQUID magnetometers is that the AM does not require cryogenic cooling. By eliminating the need for complex cryogenic equipment, AMs can substantially reduce the cost of MEG/MCG instrumentation.

AMs based on alkali atoms enclosed within a vapor cell were first developed in the 1950's (Dehmelt 1957, Bell and Bloom 1957). In 1969, Dupont-Roc and coworkers developed a zero-field version of this AM with nearly 10 fT Hz$^{-1/2}$ level sensitivity (Dupont-Roc *et al* 1969). In 1973, Tang and coworkers discovered that spin-exchange relaxation in alkali atoms

is suppressed in a low magnetic field environment, which led to miniaturization of highly sensitive AMs (Happer and Tang 1973). In 2003, Romalis and coworkers used this discovery to demonstrate an ultra-sensitive AM with sub-femtotesla level sensitivity (Kominis *et al* 2003). The AMs operating in this regime are now referred to as Spin-Exchange Relaxation-Free (SERF) magnetometers. In 2007, Shah and coworkers developed a compact version of the SERF AM, using a millimeter-scale microfabricated vapor cell and the simplified detection scheme developed by Dupont-Roc and coworkers (Shah *et al* 2007). Recently, a fully integrated version of the SERF chip-scale atomic magnetometer (CSAM) was developed at the National Institute of Standards and Technology (NIST) (Preusser *et al* 2009).

Here we describe a low-cost, compact AM that is a viable alternative to a SQUID magnetometer for biomagnetism applications requiring compact sensors with high sensitivity. Until now, AMs either lacked sufficient sensitivity or were too large and complex for biomagnetic applications. The AMs described here have size and sensitivity similar to that of SQUID magnetometers used in MEG and MCG systems, and they are manufactured using commercial off-the-shelf components with simple assembly techniques. They also have a precisely defined sensitive axis and can be integrated into a large, dense array for MEG source localization applications; thus, they are suitable as drop-in replacements for SQUID magnetometers for many biomagnetism applications.

The purpose of the study was to characterize the sensitivity and bandwidth of our AM, and to compare its performance with that of a commercial SQUID biomagnetometer by making MCG and MEG recordings in the same subjects. Similar studies using modular AMs have been recently reported by several groups. In 2009, Bison and coworkers developed a 19-channel MCG system using modular scalar AMs with 100 fT $Hz^{-1/2}$ sensitivity and a channel grid spacing of 5 cm (Bison *et al* 2009). Scalar AMs can operate in the earth's field without magnetic field compensation, but their sensitivity per unit volume is lower than that of SERF magnetometers. Another downside of a scalar magnetometer is that it measures the total magnitude of the magnetic field, making it largely insensitive to the direction of the magnetic field. This poses problems for source localization and related applications. In 2012, Wyllie and coworkers developed a four-channel MCG system, using modular two-beam vector SERF AMs with 6 fT $Hz^{-1/2}$ sensitivity and 7 cm channel grid spacing (Wyllie *et al* 2012). Johnson and coworkers have developed a similar AM with $6 \times 6 \times 20$ cm^3 outside dimensions and 6 fT $Hz^{-1/2}$ sensitivity for MEG (Johnson *et al* 2010). The chip-scale SERF magnetometer developed at NIST has the smallest footprint ($\sim 1 \times 1 \times 1$ cm^3) thus far, and under optimal conditions the sensitivity of the CSAM has been reported to be as low as 15 fT $Hz^{-1/2}$ (Mhaskar *et al* 2012).

2. Methods

2.1. Design of atomic magnetometer

The overall design and operation of our AM is similar to that of the earlier NIST CSAM that used a single optical beam. A detailed discussion of the methods can be found in (Preusser *et al* 2009, Sander *et al* 2012); only a brief summary is given here. The magnetometer consists of three main components: (i) a resonant light source, (ii) a transparent glass alkali (^{87}Rb) vapor cell, and (iii) a photodiode to monitor the intensity of the light transmitted through the vapor cell. The resonant light is generated using a narrow linewidth laser with its optical wavelength tuned to the D1 transition of ^{87}Rb atoms. The resonant light is used to spin-polarize the alkali atoms, and a zero-field cross-over resonance is observed by sweeping the magnetic field about zero in a direction perpendicular to the optical beam. A maximum in the intensity of light

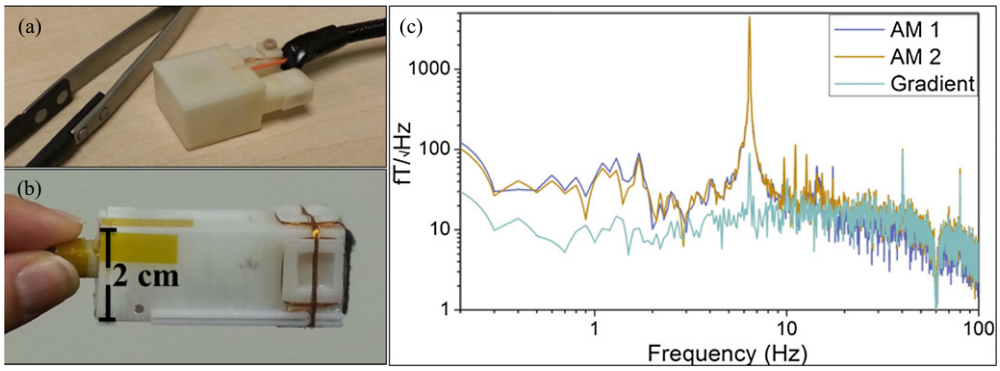

Figure 1. (a) Photograph of the prototype AM adjacent to optical tweezers. The external dimensions are 1.5 × 1.5 × 3 cm^3. (b) AM enclosed in an outer protective jacket (2 × 2 × 5 cm^3) with three-axis coils wrapped on the outside. (c) Magnetic field sensitivity of the AM prototypes. The AM1 and AM2 traces are the magnetic noise power spectral density (PSD) of the two magnetometer channels measured within the MSR at the time of AER studies, and the gradient trace is the PSD of the difference of the outputs from the two magnetometers; i.e., synthetic gradiometer. The gradiometer arrangement cancels the low frequency environmental noise inside the MSR and also removes a large interference at 7 Hz from an air conditioning fan located above the MSR. A digital notch filter was used to suppress interference at 60 Hz. The roll-off in the noise spectrum seen at frequencies above 50 Hz is due to the filter settings on the lock-in amplifier.

transmitted through the vapor cell is seen when the magnetic field is precisely equal to zero. The zero-field resonance is a Lorentzian function of the magnetic field with a full-width at half maximum of about 30 nT. The magnetometer is locked to the peak of the zero-field resonance by applying a modulation field generated by an external magnetic coil and using feedback from a lock-in amplifier.

Figure 1(a) shows a picture of our prototype AM with integrated optics, vapor cell, and photo detector. Instead of using chip-scale components, the AM here is constructed using slightly larger but lower cost off-the-shelf optical components. The 1 mm microfabricated vapor cell used in the CSAM is replaced by a 4 mm Pyrex vapor cell. The narrower resonance and stronger signals from the larger vapor cell in our AM enables the magnetometer to reliably achieve SQUID-level performance without painstaking optimization. The magnetometer housing is made using a 3D printer with high-temperature plastics. The housing has internal features that simplify the assembly process by allowing the optical components to be dropped and glued in place without manual adjustment. As shown in figure 1(a), the outside dimensions of the magnetometer are only 1.5 × 1.5 × 3 cm^3. Including the thermally insulating protective jacket, the outside dimensions are 2 × 2 × 5 cm^3 (see figure 1(b)). A set of three orthogonal magnetic coils is wrapped around the jacket to locally cancel residual magnetic fields. This eliminates the need for large external magnetic field and gradient compensation coils, allowing the magnetometer to be freely oriented in the shielded environment. The wire used to wind the magnetic coils was made from 36 AWG copper that we estimate produces magnetic Johnson noise at a level below 5 fT $Hz^{-1/2}$. A thinner or higher resistivity wire can be used to further reduce Johnson noise, if required. The typical residual magnetic field inside a MSR is less than 100 nT. The current used to drive the magnetic coils was provided by the output of a 24 bit digital-to-analog chip that was converted to a current using a metal film resistor and was heavily filtered, using a passive low pass filter. We estimate that the magnetic noise resulting from the current noise was approximately 1 fT $Hz^{-1/2}$ at frequencies above 1 Hz.

The vapor cell in the magnetometer was heated to over 150 °C to achieve sufficient alkali density to suppress spin-exchange relaxation in a low field environment. With an efficient

passive design to thermally isolate the vapor cell from the magnetometer housing, the outside surface temperature of the magnetometer rises to no more than two degrees above ambient temperature; thus, the magnetometer can be placed in proximity to or even in direct contact with the subject. The average distance between the outer surface of the AM and the center of the vapor cell is less than 1 cm. This distance is substantially shorter than the typical 2 cm distance between the SQUID coil and the outside of a SQUID dewar. The resonant light for optical pumping is delivered to the magnetometer using a polarization-maintaining fiber. Using optical fiber splitters, light from a single laser system can be distributed to multiple AM channels. The magnetic field resolution was measured separately in a three-layer, 20 cm inner diameter cylindrical μ-metal magnetic shield and inside a standard two-layer magnetically shielded room (MSR).

2.2. MCG and MEG measurements

The laboratory testing and validation of the AMs was carried out at the University of Wisconsin Biomagnetism Laboratory. MCG and auditory evoked response (AER) MEG recordings were made. For the MCG study, the subjects were ten healthy adult subjects: five male and five female. All ten subjects were studied during the same 2 h session. For the AER study, four healthy adult subjects were recorded: three male and one female. They were studied during the same 3 h session. The protocols were approved by the institutional review board, and informed consent was obtained from all subjects. The measurements were performed in a two-layer MSR (ETS-Lindgren, Glendale Heights, IL) with a dc shielding factor of about 500. The ac magnetic field attenuation was 56 dB at 0.1 Hz, 64 dB at 1 Hz, $>$85 dB at 10 Hz and above. The performance of the AMs was compared side-by-side with that of a commercial 7-vector channel SQUID magnetometer system (621 Biomagnetometer, Tristan Technologies, San Diego, CA), which records the x, y, and z components of the magnetic field at seven locations. The center channel is surrounded by six others, equally spaced on a circle with 40 cm spacing between adjacent coils. The magnetic field resolution of each channel was approximately 5 fT $\mathrm{Hz}^{-1/2}$. The channels of the Tristan 621 Biomagnetometer were configured as first-order gradiometers with 8 cm baseline. For the AMs, reference channel noise cancellation was performed by using the first AM (AM 2) as a signal channel to record MEG activity and the second (AM 1) as a reference channel to monitor the ambient magnetic interference (figure 2). The two AMs were separated by about 7 cm.

The MCG subjects lay supine on the patient table and the AM was positioned over the left ventricle at a location where the MCG signal was expected to have largest amplitude (figure 2(a)). The MCG was recorded for 1 min using a 1–100 Hz passband and 1 kHz sampling rate. Next, the SQUID magnetometer was centered at the same location, and the MCG was recorded using the same data acquisition parameters. The AM showed substantial environmental interference at several discrete frequencies including at 60 Hz. The interference signal at 60 Hz was suppressed using a real-time digital notch filter. A 4-pole, 3–43 Hz Butterworth filter was applied during post-processing. The SQUID recordings were also filtered using the same 3–43 Hz filter, although they contained much less interference since they were configured as gradiometers. Averaged MCG waveforms were computed by choosing a representative QRS complex as a template and computing the cross-correlation between the template and the MCG signal. The peaks in the cross-correlation were used to time-align the beats. All beats within a 30 s interval were used in computing the averaged waveforms. The PR, QRS, and QT intervals were measured.

The MEG subjects lay on their side and the AM was positioned over the parietal region, near an extremum of the AER (figure 2(b)). The stimuli consisted of 150 tone bursts of

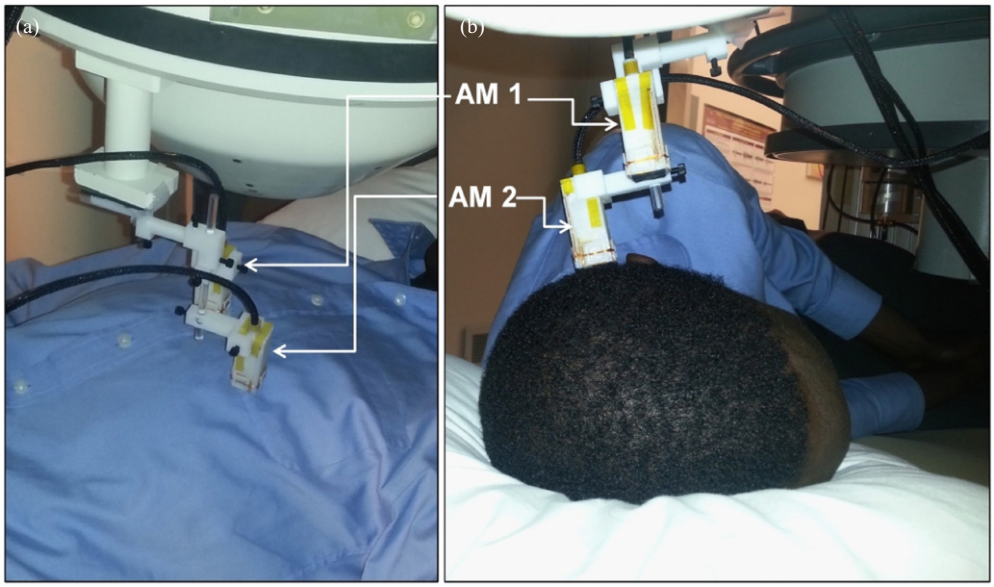

Figure 2. (a) Photograph of two AMs positioned over the chest of a subject for recording the MCG. (b) Close-up photograph of two AMs positioned over the parietal cortex for MEG-AER recordings. AM 2 was used to record the AER, while AM 1 was used as reference sensor for background noise cancellation.

frequency 1 kHz, duration 50 ms, and intensity in air of 60 dB, presented with a pseudorandom interstimulus interval of 1–3 s. The tone bursts were produced by a piezoelectric speaker placed in a small opening of the shielded room. The MEG was recorded continuously, along with a trigger, consisting of square pulses that were synchronized with the stimulus presentation. Next, the SQUID magnetometer was centered at the same location, and the MEG was recorded using the same stimulation and data acquisition parameters. Reference channel noise cancellation, as described above, was required to remove environmental noise at low frequencies, including large 7 Hz interference from a nearby air handling fan, which was turned off for the MCG study but could not be turned off for the AER study. The recordings were further band limited using a 4-pole 3–48 Hz Butterworth filter. The SQUID recordings were also filtered using the same 3–48 Hz filter. Averaged AERs were computed, using the trigger channel to time-align the 150 AERs. In addition to recording AERs, in one subject the spontaneous MEG was recorded with the AM positioned over the occipital cortex. The subject was instructed to open and close his eyes in order to demonstrate blocking of the alpha rhythm.

3. Results

Figure 1(c) shows the sensitivity of two of the AM prototypes placed adjacent to each other in the MSR just prior to the AER studies. By using the standard technique of forming a gradiometer by subtracting the common mode signal, we were able to recover the true sensitivity of the AM inside the MSR. The true sensitivity of each of the two magnetometers was around 10 fT $Hz^{-1/2}$ and could be reliably reproduced. Under optimal conditions in the laboratory, the AM sensitivity reached 6 fT $Hz^{-1/2}$. The environmental magnetic noise inside the MSR limited the sensitivity of the AMs at low frequencies. The 3 dB bandwidth of the AM was roughly 100 Hz, which is sufficient for most MEG and MCG applications.

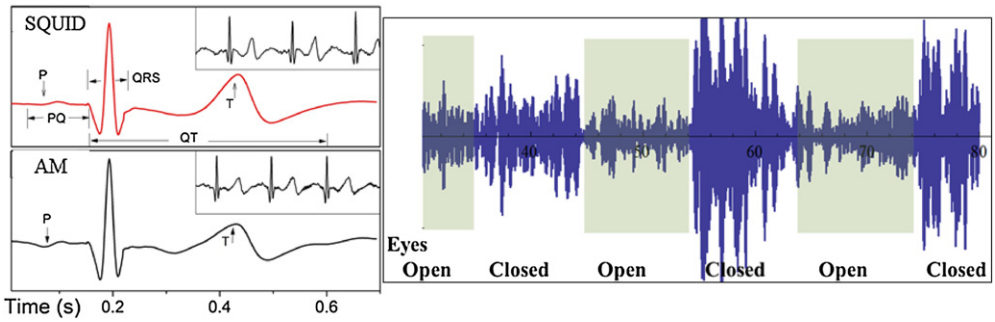

Figure 3. Left: signal-averaged MCG waveforms from subject #1, obtained using the SQUID and AM. The peak-to-peak amplitude of the signal is about 75 pT. The insets show the raw recordings, except for application of a 60 Hz notch filter. Right: 8–12 Hz MEG recording showing blocking of the alpha rhythm, obtained by instructing the subject to alternately open and close his eyes every ten seconds.

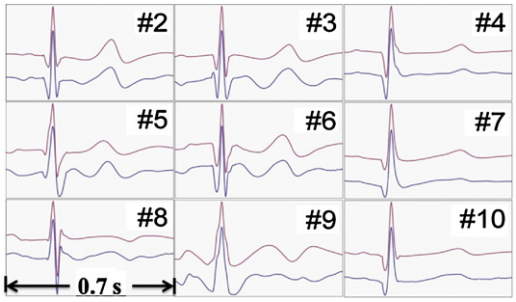

Figure 4. Averaged MCG waveforms from nine subjects, recorded with a SQUID (red) and AM (blue). The *x*-axis in each of the plots is time (0.7 s full-scale). The *y*-axis is magnetic field, arbitrarily scaled to facilitate comparison.

Figure 3(a) shows a side-by-side comparison of averaged MCG waveforms from an adult subject, acquired successively with the AM and the SQUID magnetometer. The SQUID data are from a channel with large amplitude that most closely resembled the AM data. The waveforms registered by the two systems were very similar in overall quality. They are also remarkably similar in morphology, given that the position and orientation of the magnetometers were only approximately the same and that the AM and the SQUID magnetometer measure the magnetic field and the magnetic field gradient, respectively. The inset in figure 3(a) shows the raw, full bandwidth MCG trace after application of only a 60 Hz notch filter. Equally high quality signals were obtained from all ten subjects. In figure 4, similar side-by-side comparisons of time averaged MCG recordings are shown for the other nine subjects. The cardiac waveform intervals obtained with the two systems were also highly consistent. The limits of agreement were $\leqslant$5 ms for QRS interval, $\leqslant$10 ms PR interval and $\leqslant$25 ms for QTc interval. These limits are small enough that the differences in the measurements are not considered clinically significant.

Figure 3(b) shows a 8–12 Hz filtered MEG recording that depicts the phenomenon of alpha blocking, in which the alpha rhythm is diminished when the subject opens his eyes.

Figure 5 shows a comparison of AERs recorded using the SQUID magnetometer and AM in four subjects. The left graph for each subject in figure 5 shows a superimposition, or 'butterfly', plot of the SQUID channels. The right graph shows a comparison between the

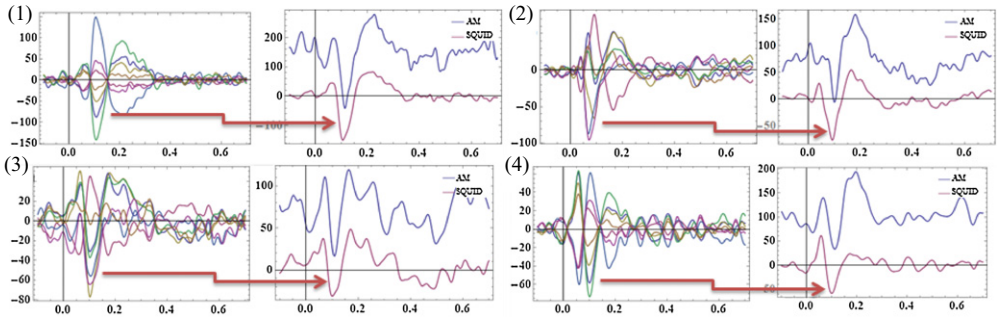

Figure 5. Averaged AER recordings made using a SQUID and AM. The left graph for each of the four subjects is the AER recorded using a seven-channel vector SQUID system. Right: comparison of AERs measured using the AM (blue) and a SQUID channel (red) with similar morphology. The *x*-axis shows time in seconds and the *y*-axis shows magnetic field in fT. The SQUID and AM recordings were vertically offset to facilitate comparison.

response from the AM and the response from a representative SQUID channel with similar morphology. Again, the AM and SQUID recordings are very similar in quality and appearance.

4. Discussions

The data presented here validate the excellent performance of our AM. Both the MCG and MEG data obtained with our AM were remarkably similar in morphology and quality to data obtained with a SQUID magnetometer. In previous MEG studies using modular AMs, Sanders and coworkers and Johnson and coworkers achieved sensitivity of 200 and 50 fT $Hz^{-1/2}$, respectively, with an average distance from the center of the sensing volume (vapor cell) to the scalp of 0.5 and 2.5 cm, respectively. With the higher sensitivity of our AM and a shorter distance to the body surface, we were able to achieve sufficiently high signal-to-noise ratio by averaging just 150 trials, which is typical for an MEG studies using SQUID magnetometers.

The magnetic field resolution of our AM was around 10 fT $Hz^{-1/2}$ during the AER study and around 6 fT $Hz^{-1/2}$ in the laboratory, whereas commercial SQUID magnetometers in MEG/MCG systems typically achieve a resolution of 3–4 fT $Hz^{-1/2}$. In the laboratory, the SQUID magnetometers have reached sensitivity as high as 0.9 fT $Hz^{-1/2}$ (Drung 2002). In comparison, the theoretical atomic shot noise limited sensitivity of our AM was $<$0.1 fT $Hz^{-1/2}$, and the photon shot noise limited sensitivity was around 1 fT $Hz^{-1/2}$ (Shah and Romalis 2009). In the future, we believe photon shot noise limited sensitivity can be reached with our AM without significantly modifying its design, through optimization and improvements in laser stabilization.

One important difference between a SQUID magnetometer and an AM is that the SQUID magnetometer's pickup coil can be wound to configure the device as a gradiometer, which greatly improves rejection of environmental interference. Using AMs, however, gradiometers are much more difficult to implement and instead a separate calibrated reference channel is required for noise cancellation, as demonstrated here.

The frequency response of the AM is given by the square root of a Lorentzian function, $s(f) = s0/[1+(2\pi f T_2)^2]^{1/2}$, where the width is determined by the inverse of the spin coherence time, T_2. The 3 dB bandwidth of our AM was roughly 100 Hz, corresponding to a $T_2 \sim$ 2 ms. For some MEG applications that require bandwidth greater than 100 Hz, it is possible to make trade-offs between sensitivity and bandwidth by intentionally broadening the atomic

resonance. In an optimized system, the AM sensitivity decreases as the square root of the AM bandwidth.

The intrinsic dynamic range of a SERF AM is approximately equal to the half-width of the zero-field resonance, which in our AM was 15 nT; however the effective dynamic range can be made arbitrarily large by applying feedback. Magnetic coils were wound on the magnetometer to locally compensate the magnetic field in the vicinity of the vapor cell. Using feedback, the external coils can be locked to the peak of the atomic resonance to ensure that magnetic field in the vicinity of the vapor cell remains close to zero. To minimize cross-talk arising from fields generated by the compensating coils on adjacent magnetometers, the feedback time constant for the coils can be made sufficiently large to correct only slow drifts in the field inside the shielded environment, thereby minimizing inference from external coils over time scales relevant to the measurement.

AMs do not require equipment for cryogenic cooling, which is the main expense in a SQUID-based biomagnetic system. Another potential advantage of an AM system is its small overall size. Because a bulky cryogenic dewar is not needed, it should be possible to make measurements in compact human-sized cylindrical shields that cost nearly an order of magnitude less than a typical MSR. Xia and coworkers have shown that human studies can be made conveniently in compact cylindrical magnetic shields using AMs (Xia *et al* 2006), which is challenging with SQUID systems (Seki *et al* 2005).

Although we have demonstrated only single-channel MCG/MEG, we believe the AMs described here satisfy all the requirements for incorporation into multi-channel MCG and whole-head MEG systems: (i) The AMs described here are sufficiently compact for constructing MCG arrays and MEG helmets with high channel density. (ii) The sensitive axis of the AMs is along the long axis of the magnetometer. This allows the AMs to be closely spaced to measure the radial component of the magnetic field, which is the most important component. (iii) The position and orientation of each magnetometer channel can be precisely known, which is crucial for source localization and quantitative measurements as well as environmental noise cancellation. This is accomplished through the use of a modulation field produced by a magnetic coil wrapped on the jacket of the magnetometer, which precisely defines the sensitive axis of the magnetometer. (iv) Synthetic gradiometers can be formed to improve rejection of environmental interference by deploying three orthogonal AMs to serve as reference channels.

Currently, AMs cannot be used as direct replacements for SQUIDs for all applications because they have lower bandwidth and lose sensitivity if operated outside a low field environment; however, the AM demonstrated in this study fulfills the principal requirements that will allow its use for most biomagnetism applications. In the near future we plan to construct a large multi-channel array suitable for such applications as fetal and adult MCG.

Acknowledgments

This work was supported by the NIH grants R43 HD074495 and R01 HL063174.

References

Bell W E and Bloom A L 1957 Optical detection of magnetic resonance in alkali metal vapor *Phys. Rev.* **107** 1559

Bison G, Castagna N, Hofer A, Knowles P, Schenker J-L, Kasprzak M, Saudan H and Weis A 2009 A room temperature 19-channel magnetic field mapping device for cardiac signals *Appl. Phys. Lett.* **95** 173701

Dang H B, Maloof A C and Romalis M V 2010 Ultrahigh sensitivity magnetic field and magnetization measurements with an atomic magnetometer *Appl. Phys. Lett.* **97** 151110

Dehmelt H G 1957 Modulation of a light beam by precessing absorbing atoms *Phys. Rev.* **105** 1924

Drung D 2002 High-performance DC SQUID read-out electronics *Phys. C Supercond.* **368** 134–40

Dupont-Roc J, Haroche S and Cohen-Tannoudji C 1969 Detection of very weak magnetic fields (10−9gauss) by 87Rb zero-field level crossing resonances *Phys. Lett.* A **28** 638–9

Happer W and Tang H 1973 Spin-exchange shift and narrowing of magnetic resonance lines in optically pumped alkali vapors *Phys. Rev. Lett.* **31** 273

Johnson C, Schwindt P D D and Weisend M 2010 Magnetoencephalography with a two-color pump-probe, fiber-coupled atomic magnetometer *Appl. Phys. Lett.* **97** 243703

Kominis I K, Kornack T W, Allred J C and Romalis M V 2003 A subfemtotesla multichannel atomic magnetometer *Nature* **422** 596–9

Mhaskar R, Knappe S and Kitching J 2012 A low-power, high-sensitivity micromachined optical magnetometer *Appl. Phys. Lett.* **101** 241105

Preusser J, Knappe S, Gerginov V and Kitching J 2009 A microfabricated photonic magnetometer *EQEC 2009: European Conf. on Lasers and Electro-Optics 2009 and the European Quantum Electronics Conf. (Munich, Germany, 14–19 June 2009)* p 1

Sander T H, Preusser J, Mhaskar R, Kitching J, Trahms L and Knappe S 2012 Magnetoencephalography with a chip-scale atomic magnetometer *Biomed. Opt. Express* **3** 981–90

Seki Y, Kandori A, Suzuki D and Ohnuma M 2005 Open-type magnetocardiograph with cylindrical magnetic shield *Appl. Phys. Lett.* **86** 243902

Shah V, Knappe S, Schwindt P D D and Kitching J 2007 Subpicotesla atomic magnetometry with a microfabricated vapour cell *Nature Photon.* **1** 649–52

Shah V and Romalis M V 2009 Spin-exchange relaxation-free magnetometry using elliptically polarized light *Phys. Rev.* **80** 013416

Weinstock H 1996 *SQUID Sensors: Fundamentals, Fabrication and Applications (NATO Science Series E)* 1st edn (Berlin: Springer)

Wyllie R, Kauer M, Smetana G S, Wakai R T and Walker T G 2012 Magnetocardiography with a modular spin-exchange relaxation-free atomic magnetometer array *Phys. Med. Biol.* **57** 2619–32

Xia H, Ben-Amar Baranga A, Hoffman D and Romalis M V 2006 Magnetoencephalography with an atomic magnetometer *Appl. Phys. Lett.* **89** 211104